Modeling Mass Transfer During Single Organic Droplet Formation and Rise

Esko Lahdenperä*, Jussi Tamminen, Tuomas Koiranen, Toni Kuronen, Tuomas Eerola, Lasse Lensu and Heikki Kälviäinen

School of Engineering Science, Lappeenranta University of Technology, Lappeenranta, Finland

Abstract

Copper reactive extraction from ambient aqueous solution to organic droplets using single droplet experiments was performed. Extractant was Agorca M5640 hydroxyoxime in Exxsol D80. An image analysis based method was used to determine droplet concentration directly after droplet formation and rise. Mass transfer during formation is correlated using literature. Level Set interface tracking method was used to find formation hydrodynamics and as a result the assumption of non-circular velocity field could be validated. This was also supported by the circulation criteria based on needle Reynolds number. A model to estimate extraction rate as function of droplet Fourier number was based on a literature correlation and it was found that a model where the interface effect was described using interface mobility parameter was able to predict satisfactorily mass transfer. For a rising droplet stagnant cap model was used. Stagnant cap volumes were estimated from droplet images. A CFD model of a non-deforming rising droplet with rigid interface was used to fit interfacial reaction kinetic constant. Fitted value was much lower than experimentally determined by high a shear reactor. Mass transfer coefficients calculated from CFD model and estimated using literature correlations agreed well. By applying a two-film model it was shown that major part of the resistance is located at the interface between the phases.

Keywords: Mass transfer; Copper extraction; Liquid-liquid extraction; Mathematical model; CFD

Introduction

Single droplet experiment is a common method to determine mass transfer rates between the feeds in liquid-liquid extraction (LLE). During a single droplet experiment three stages are identified: (1) droplet formation, detachment and acceleration, (2) droplet rise/fall and (3) droplet coalescence [1]. In traditional experiments a droplet concentration are measured before formation and after coalescence and this provides an overall mass transfer rates for all stages. By using suitable experimental arrangements the effect of coalescence can be minimized but the droplet formation stage is often substantial [2-5] and by using several different droplet rise times the effect of formation is found by extrapolation of results into zero rise time.

This indirect method to determine the amount mass transfer during formation has some drawbacks. Application of the method requires several experimental points in order to get statistically relevant results. In this work this problem is avoided by using an image analysis based direct measurement method developed by Tamminen et al. [6] to measure concentrations directly from the column. This also simplifies experimental setup as there are no strict limitations for the coalescence stage arrangements.

Mass transfer correlations during droplet formation correlate the amount of extracted Δn or the extraction ratio E as a function of Fourier number $FO_d = 4D_m t_F / d_e^2$ [7-10]. Diameter d_e is volume equivalent sphere diameter after droplet formation. Those correlations assume that mass transfer inside the droplet is purely diffusion based. To take into account the intensifying effect of internal circulation and the hindering effect of surfactants, Liang and Slater [4] formulated overall effective diffusivity $D_{F,eff} = k_{H,F}(D_m + D_{E,F})$ where $D_{F,E}$ is time dependent diffusivity due to circulation. The empirical parameter $k_{H,F}$ takes into account the effect of surfactants. Depending on the interface properties, $k_{H,F}$ varies between 0 and 1. Liang and Slater [4] also propose a criterion based on the needle Reynolds number, whether there is circulation during droplet formation.

Kumar and Hartland [11] have published a collection of mass transfer correlations for a rising droplet. For the continuous phase correlations are expressed in form $Sh_C = f(Re, Sc_c, K)$ where K is viscosity ratio between dispersed and continuous phase. Droplet side correlations are based on Newman [12] model, which assumes no circulation. The intensifying effect of droplet internal circulation is taken into account by (1) using the effective diffusion coefficient D_{eff} which is D_m multiplied with a constant [12,13], (2) using eddy diffusivity D_E [14] or (3) combining eddy and molecular diffusivities into an effective diffusivity D_{eff} [15-17]. To take into account the effect of surfactants, Slater [18] applied the stagnant cap model where a droplet is divided into a circulating and stagnant regions. Effect of surfactants on interface mobility is implemented by using a similar experimental parameter $k_{H,R}$ as was used in droplet formation.

DNS (=Direct Numerical Simulation) method to solve transport equations can, in principle, provide parameters for the constitutive equations, like mass transfer coefficients. During droplet rise, if a droplet is smaller than the critical diameter then it maintains sphericity and it can be modelled as a sphere with constant shape and diameter. This approach has been used by Piarah et al. [19], Wegener et al. [20], Jeon et al. [21] and Pawelski et al. [22]. When a droplet is deformed due to diameter being larger than critical diameter, interface tracking offers a method to model the combined effect of hydrodynamics and interface evolution on mass transfer. A rising droplet interface tracking has been applied by, for example, Deshpande and Zimmerman [23],

Citation: Lahdenperä E, Tamminen J, Koiranen T, Kuronen T, Eerola T, et al. (2018) Modeling Mass Transfer During Single Organic Droplet Formation and Rise. J Chem Eng Process Technol 9: 378. doi: 10.4172/2157-7048.1000378

Yang and Mao [24], Kenig et al. [25] and Wang et al. [26] who all have used Level Set (LS) method. For the droplet formation, LS method is used by Lu et al. and Soleymani et al. [27,28]. Soleymani et al. however, model only droplet hydrodynamics during formation and rise and they do not calculate mass transfer.

When the classical two-film theory is used to describe mass transfer between two feeds LLE, it is assumed that two films having finite thickness is formed between the phases. The interface itself is assumed to have infinitely small width thus providing negligible mass transfer resistance [29]. However, the assumption of negligible interface thickness and resistance is questionable [30]. Hu et al. [31] modelled mass transfer in LLE using molecular simulation and according to their result, as a contrary to assumption used in two-film theory, the effect of the interface on the mass transfer cannot be neglected. Hu et al. also claim that the surfactants restructure the interface and the mass transfer mechanism is modified. An additional component to be considered is an interface reaction which in two-film theory is assumed to be a surface phenomenon and proceeding with the kinetics of its own. But according to Hu et al. the interface structure is complex and it can be assumed that the empirical parameters for reaction kinetic models determined, for example, in high shear mixers, are not usable because of missing interface effects.

In this study the focus is on mass transfer from continuous phase to organic droplet. Models of copper reactive extraction from aqueous phase into an organic droplet during droplet formation and droplet rise were formulated. Droplets were formed using 0.4 and 0.8 mm needles with several different feed rates. Droplet concentrations, diameters and velocities after the formation and in the end of the rise were measured with an image analysis method. The method is documented in the previous work by Tamminen et al. [6]. An empirical model of mass transfer in droplet formation is based on a methodology proposed by Walia and Vir [9] enhanced by Liang and Slater [4]. Results are compared with Popovich [7] model. The droplet formation hydrodynamics is simulated with CFD using LS method to provide support for the selected velocity profile during droplet formation.

Copper transport from aqueous continuous phase to the organic droplet during droplet rise was modelled with CFD using a stationary spherical droplet with non-deforming interface. The ambient aqueous phase is moving with the measured droplet terminal velocity. Stagnant cap model was implemented by dividing the droplet interface into two domains. Velocity boundary condition was used to adapt corresponding interface mobility to reflect stagnant cap properties. By assuming a fully rigid interface (k_{HR}=0) the reaction kinetic coefficient and extraction rate were estimated. Fractional mass transfer resistances were calculated from the film model.

Materials and Methods

Experiments

Experiments were made using same feeds, setup and method as in previous work by Tamminen et al. [6]. Results of previous work were extended here by using a smaller diameter needle (0.4 mm) in drop formation.

The droplet formation flow rates were 0.041, 0.21, and 0.29 mL/min in case of 0.4 mm needle and 0.10, 0.30, 0.50, 0.70 mL/min, when 0.8 mm needle was used. Needle Reynolds number Re_N was between 1-10. Droplet formation times were not explicitly measured. They were calculated based on feed rate and measured droplet volume.

Contact angles were measured from sessile droplets with 20 vol-% Acorga M5640 in Exxsol D80 (by Exxon). The aqueous phase was 0.16 M copper sulfate solution. The size of droplet and the height (h) of a sessile droplet from needle tip to droplet apex were measured. Contact angle is calculated from $\tan(\theta/2) = h/r_d$ [32]. Droplet image axes measured in x- and y-directions confirmed spherical droplet assumption. Estimated contact angle θ is 120° Measured physical properties of 20 vol-% Agorca solution are shown in Tables 1 and 2.

Details of feed solution preparation, experimental arrangement, droplet imaging and analysis method are documented [6]. Local droplet concentrations were measured at the end of the droplet rise and just after the droplet detachment.

Mass transfer in droplet formation

Popovich [7] has presented a model to describe the total mass transfer during droplet formation:

$$\Delta n = a_1(c_d^* - c_{d,o})\sqrt{\pi D_m t_F d_e^{\,2}} = a_1(c_d^* - c_d)\frac{de}{2}\sqrt{\pi Fo_d d_e^{\,2}} \quad (1)$$

Where c_d^* is equilibrium concentration, $c_{d,O}$ is initial concentration and t_F is the formation time of a spherical droplet having volume equivalent diameter d_e. The model is based on assumption that the mass transfer process is diffusion controlled so interfacial instabilities and internal circulation is not taken into account. The constant a_1 varies between 0.857 and 3.43 [5].

In the model by Liang and Slater [4] the extraction ratio E is calculated with the model developed by Walia and Vir [8,9]

$$E = E_d - (7/8)E_d^2 + (49/72)E_d^3 - 0.476E_d^4 \quad (2)$$

Liang and Slater [4] define the term E_d as a function of modified Fourier number Fo'_d

$$E_d \frac{36}{\sqrt{21\pi}} \frac{1}{2}\sqrt{Fo'_d}(1 + \frac{1}{2}\sqrt{\pi Fo'_d}) \quad (3)$$

Modified Fourier number Fo'_d uses overall effective diffusivity $D_{F,eff}$ instead of molecular diffusivity D_m The overall effective diffusivity is defined as:

$$D_{F,eff} = k_{H,F}(D_m + D_{F,E}) \quad (4)$$

Where $k_{H,F}$ describes the effect of surfactant and has values between 0 to 1, and $D_{F,E}$ is pseudo-eddy diffusivity to take into account the effect of droplet internal circulation. Liang and Slater [4] propose a method to judge if system is (1) diffusion controlled Re_N<10, or (2) circulation enhanced diffusion: 10<Re_N<34, or (3) circulation controlled: 10<Re_N>34. In a system with pure diffusion control, the diffusivity D_m is to be used. In cases 2 and 3 the enhancing effect of circulation on the mass transfer is taken into account using $D_{F,E}$.

Liang and Slater [4] considered only interfacial effects to be included in the constant $k_{H,F}$ but also other effects like the resistance generated by interfacial reaction can also taken into account [33,34].

Mass transfer during droplet rise

When a droplet is rising the mass transfer is affected by diffusion and internal circulation and also the outside convection as well. Depending on the interface mobility, the interface can be rigid or mobile and this has an effect on droplet internal circulation strength.

Correlations provided by the literature are mostly for systems without contaminations and surfactants [11]. Slater [18] has formulated

a model to take into account decrease of mass transfer rates due to surface effects and defines a correction factor $K_{H,R}$:

$$k_{H,R} = \overline{U}_i / U_t \qquad (5)$$

Where $\overline{U}_i$ is the average interfacial velocity and is U_t droplet terminal velocity.

The stagnant cap model for a rising droplet by Slater [18] is applied. The model is based on the concept of two zones, where one zone is stagnant and another zone is circulatory (Figure 1). Surfactants and other contaminants act against circulation and as a result the interface becomes more rigid [18].

A droplet is divided into two zones having relative sizes f_v and $1-f_v$, where f_v is size of the stagnant zone. An overall effective diffusivity is calculated based on f_v, molecular diffusivity D_m and eddy diffusivity $D_{R,E}$.

$$D_{R,eff} = f_v D_m + (1-f_v)(D_m + D_{F,E}) \qquad (6)$$

Eddy diffusivity describes the effect of internal circulation on mass transfer and is calculated using Handlos and Baron Method [14]:

$$D_{R,E} = \frac{k_{H,R} U_t d_e}{2048(1 + \mu_d / \mu_c)} \qquad (7)$$

It can be assumed that in this system the interface is rigid so $k_{H,R}=0$. Droplet phase mass transfer coefficient is calculated using the model by Newman [12]. The overall effective diffusivity defined in eq. (7) is used here:

$$k_{CuA2} = -\frac{d_e}{6t_R} \ln\left(\frac{6}{\pi^2}\right) \sum_{z=1}^{\infty} \frac{1}{Z^2} \exp\left(-\frac{4z^2\pi^2 D_{R,eff} t_R}{d_e^2}\right) \qquad (8)$$

This equation is valid for a case where the main mass transfer resistance is on the droplet side [18].

Stagnant zone size was estimated from droplet concentration distribution images. An example of concentration profiles in a rising droplet is shown in Figure 2. The average overall mass transfer coefficient K_d during droplet rise is:

$$K_d = -\ln\left(\frac{c_d^* - c_d}{c_d^* - c_{d,0}}\right) \frac{d_e}{6t_R} \qquad (9)$$

Where t_R is droplet rise time and $c_{d,O}$ is droplet concentration after formation. This equation can be used as well to calculate mass transfer coefficient during formation. The time to use, then, is the droplet formation time t_F and $c_{d,o}$ is feed concentration which in most cases is zero [35].

CFD model for droplet formation

Droplet coalescence simulations were performed with Comsol Multiphysics v.5.2 [36] using LS method for two-phase laminar flows. A 2-d axisymmetric geometry was used. Geometry and boundary conditions are shown in Figures 3a and 3b. Two needle diameters were used: 0.8 mm o.d/0.51 mm i.d and 0.41 mm o.d and inner diameter 0.21 mm. Calculation domain dimensions were 3.8 mm width and height 10.2 mm. Same domain size was used for both needles.

A hemisphere having diameter of needle inlet was formed before calculations (Figure 3b). Initially both phase velocities and pressures were set to 0. The Comsol LS solver performs a steady state calculation at time $t=0$ to get consistent initial state for the transient calculation.
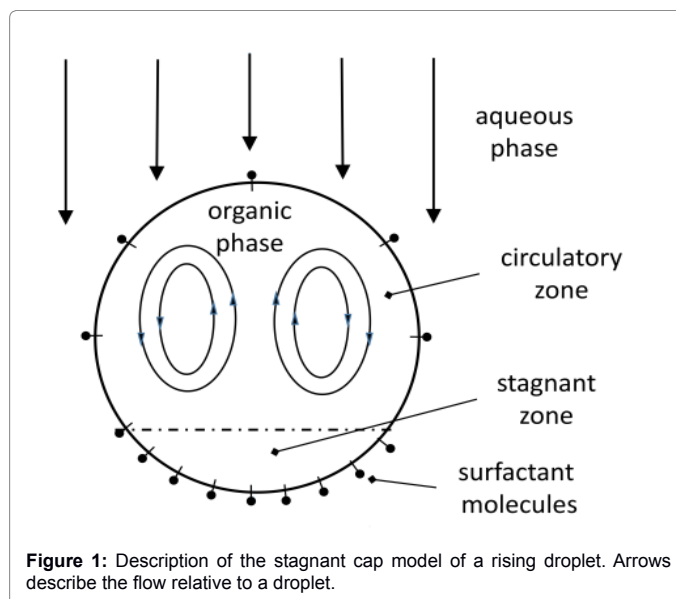

Figure 1: Description of the stagnant cap model of a rising droplet. Arrows describe the flow relative to a droplet.
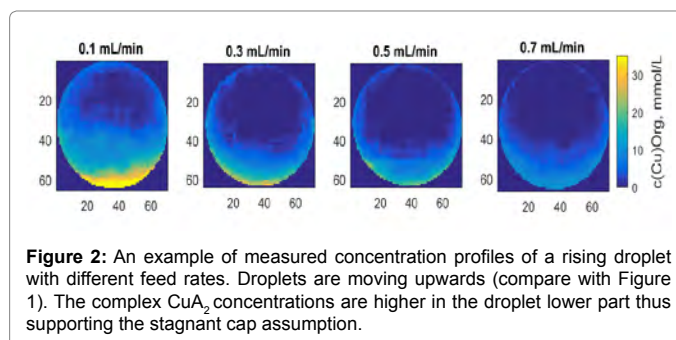

Figure 2: An example of measured concentration profiles of a rising droplet with different feed rates. Droplets are moving upwards (compare with Figure 1). The complex CuA_2 concentrations are higher in the droplet lower part thus supporting the stagnant cap assumption.
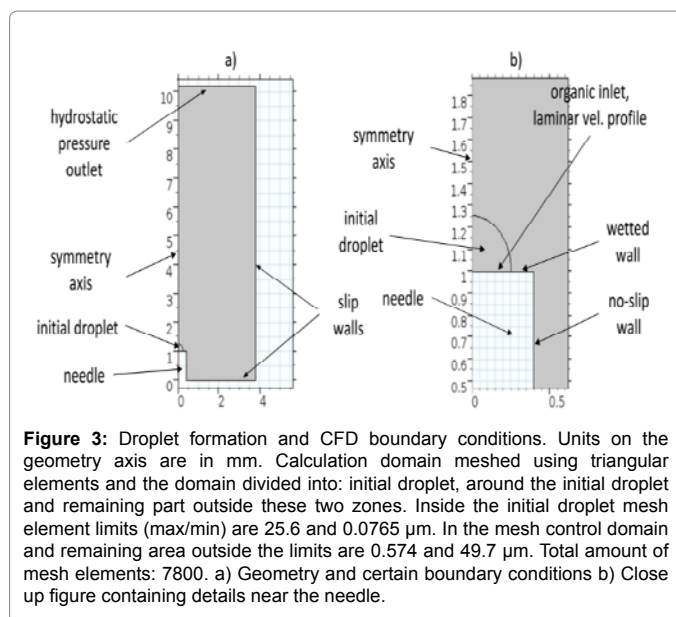

Figure 3: Droplet formation and CFD boundary conditions. Units on the geometry axis are in mm. Calculation domain meshed using triangular elements and the domain divided into: initial droplet, around the initial droplet and remaining part outside these two zones. Inside the initial droplet mesh element limits (max/min) are 25.6 and 0.0765 µm. In the mesh control domain and remaining area outside the limits are 0.574 and 49.7 µm. Total amount of mesh elements: 7800. a) Geometry and certain boundary conditions b) Close up figure containing details near the needle.

The default LS solver was used. Two user controllable LS parameters, reinitialization parameter and interface thickness parameter were adjusted to reach convergence. Reinitialization parameter was set to 0.1 ms^{-1} and interface thickness was half of the maximum element size.

CFD model for droplet rise

Mass transfer between the continuous phase and droplet was calculated with a CFD-model using Comsol Multiphysics v.5.2 [36]. The surface velocity correction factor $k_{H,R}$ was determined with this model to take into account the drag increasing effect of surface active agents, local mass transfer coefficients K_{cu} and k_{CuA2} of Cu transfer in continuous phase and in droplet (eqs. 12b, 12c) and the overall mass transfer coefficient K_D (eq. 12a).

The system is modeled as a stationary spherical droplet and the continuous aqueous phase is moving with a measured terminal velocity. Both phases are separate calculation domains. The following assumptions are used: 2-d axisymmetric geometry, the spherical droplet, laminar velocity fields, steady and constant droplet volume.

Droplet was divided into two domains: stagnant cap zone having volume fraction of f_v and circulating zone with $1-f_v$ volume fraction.

The rectangular continuous phase domain width and height were set to 3 and 10 times the droplet diameter, respectively. Unstructured triangular mesh was used for the droplet and continuous phase domains. The fine grid resolution along the interface was created by specifying the amount of cells at the interface. Mesh sensitivity was tested by refining the grid near the interface. Variation of mass transfer coefficient was used as criteria for grid independence. Calculation was performed in two stages. In the first stage, laminar Navier-Stokes equation was solved to provide flow field. Boundary conditions for the continuous phase were: uniform velocity U_t at inlet, which is the experimentally determined droplet terminal velocity; sliding wall at calculation domain vertical sides; uniform velocity U_t at outlet. At droplet side $p=0$ as a pressure constraint; sliding wall with tangential velocity set to average interface velocity $\overline{U_i} = k_{H,R}U_t$ at droplet interphase; full rigid interface is simulated by setting $K_{H,R}$ to 0.

Boundary conditions for the droplet phase were: moving wall with radial velocity $u_d=u_c$ and axial velocity $w_d=w_c$ at droplet and continuous phase interface pressure is equal to pressure on the continuous side as pressure constraint. Species diffusivities presented in Table 2.

Boundary condition between organic and droplet phases is set by the interfacial reaction rate. The extraction of copper with a hydroxyoxime HA at the phase interface [37-39] is:

$$Cu^{2+}(aq)+2HA(org) \rightleftharpoons 2H^+(aq)+CuA2(org) \quad (10)$$
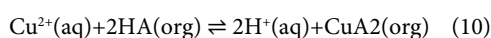
and the reaction rate equation is:

$$R_A(t) = k_{R,A} \frac{[Cu^{2+}(i)][HA(i)]^2}{[H^+(i)]} + \frac{k_{R,A}}{K_E}[CuA_2(i)][H^+(i)] \quad (11)$$

Where R_A is area based reaction rate, $k_{R,A}$ kinetic constant, K_E equilibrium constant and $[Cu^{2+}(i)]$, $[HA(i)]$, $[H^+(i)]$ and $[CuA2(i)]$ are concentrations at the interface. Tamminen et al. [38] determined kinetic constant in a high shear reactor: $k^0_{R,A}=1.4 \times 10^{-3}$ dm^4 /(mol s). Equilibrium constant k_E is 8 at hydroxyoxime concentration 20vol-%=0.38 M [39]. In this work due to very mild hydrodynamic conditions, the expected kinetic constant will be lower than determined in the high shear experiments.

Overall mass transfer coefficient, K_d and local mass transfer coefficients on droplet and continuous phase side kcuA2 and k_{cu} are determined from:

$$K_d = \frac{V_d([CuA_2](t_R)-[CuA_2]_F)}{A_d \int_0^{t_R} \{[CuA_2]^*-[CuA_2](t)\} dt} \quad (12a)$$

$$k_{cu} = \frac{V_d([CuA_2](t_R)-[CuA_2]_F)}{A_d \int_0^{t_R} \{[Cu^{2+}]-[\overline{Cu^{2+}(i)}](t)\} dt} \quad (12b)$$

$$k_d = k_{cuA_2} = \frac{V_d([CuA_2](t_R)-[CuA_2]_F)}{A_d \int_0^{t_R} \{[\overline{CuA2(i)}](t)-[CuA_2]\} dt} \quad (12c)$$

$\overline{[CuA_2(i)]}$ and $\overline{[Cu^{2+}(i)]}$ are average concentrations at the phase interface.

Results and Discussion

The estimation and application of mass transfer models are described in Figure 4.

Droplet formation

In Table 3 is shown droplet experiment results. Droplet volumes were calculated using formula:

$$V_d=(\pi/6)d^2_{Maj}d_{Min} \quad (13)$$

Average droplet volumes were 29 mm^3 for the 0.8 mm needle and 10 mm^3 for the 0.4 mm needle and corresponding average volume equivalent diameters d_e were 3.8 and 2.7 mm. Droplet average formation times t_F were estimated by dividing the average droplet volume with a feed rate: for the 0.8 mm needle 16, 5, 3 and 2 seconds and for the 0.4 mm needle 21, 4 and 3 seconds.

In Figure 5 is plotted the cumulative mass transfer Δn against the Fourier number and the and the cumulative transfer model by Popovich (eq. 1). The estimated value of the coefficient a_1 is 0.35. This is smaller than the minimum 0.857 noted by Wegener et al. [5] which confirms that in addition to diffusion there are other phenomena

X$_{HA}$	C$_{HA}$	ρ	μ	γ	Θ
vol-%	M	kg/m^3	mPas	mN/m	degrees
20	0.38	834	3	21.6	120

Table 1: The measured physical properties of Acorga M5640 solutions dissolved in Exxsol D80. Measurements at room temperature (22-24°C). Interfacial tension measured in 0.16 M CuSO$_4$ solution. pH of copper sulphate solution was adjusted to 3.1 with concentrated sulphuric acid.

Species	Cu^{2+}	H$^+$	HA	CuA$_2$
D$_m$/10^{-9} m^2/s	0.72	9.4	0.46	0.3

Table 2: Species molecular diffusivities in 25°C, Cu^{2+} and H$^+$ diffusivities are from Haynes [33], CuA$_2$ diffusivity and hydroxyoxime HA were estimated by Wilke-Chang method [34,35].

d$_N$	Q	d$_{Maj}$	D$_{Min}$	V$_d$	c$_{F,m}$	Re$_N$
mm	mL/min	mm	mm	mm^3	Mmol^{-1}	
0.8^a	0.1	3.9	3.3	26	5.3	1.2
	0.3	3.9	3.4	27	1.7	3.4
	0.5	3.9	3.3	26	1	5.7
	0.7	3.8	3.2	24	0.8	8
0.4^b	0.04	3.1	2.7	14	6.1	1.1
	0.21	3	2.6	12	1.8	5.7
	0.29	3.3	20.8	16	1.3	8.0

Table 3: Measured droplet dimensions and concentrations with different feed rates Q after droplet formation. Symbols: d$_N$, needle diameter, d$_{Maj}$, d$_{Min}$, droplet major and minor axes lengths, V$_d$, droplet volume c$_{F,m}$, measured droplet concentration, Re$_N$, Reynolds number in needle outlet.

(interfacial reaction combined with effect of surfactants) and Popovich model does not follow experimental points.

In Figure 6 is plotted extraction ratio E versus square root of droplet modified Fourier number Fo'_d using Walia and Vir model (eq. 2) with the overall effective diffusivity $D_{F,eff}$ using eq. (4). The fitted values of the surface mobility correction factor $k_{H,F}$ are 0.070 (R^2=0.76) for the 3.8 mm and 0.071 (R^2=0.90) for the 2.7 mm droplets and they are practically equal. The needle Reynolds numbers (Table 3) are less than 10 and according to the criteria proposed by Liang and Slater [4], droplet internal mass transfer is diffusion controlled. Therefore the eddy diffusivity was set to zero and the molecular diffusivity was used in calculation of the overall effective diffusivity. Compared to Popovich model Walia-Vir model combined with effective diffusivity model by Liang and Slater [4] is able to better describe mass transfer during droplet formation.

LS simulation and non-circular assumption

The non-circulatory assumption and the effect of contact angle on the formation hydrodynamics was examined by simulation of droplet formation with three different contact angles using LS method for the studied chemical system. Angles in simulations were 1, 120 and 179 degrees. Based on the simulation results shown in Figure 7 the velocity streamline profile is non-circulatory with the measured θ=120°. When the contact angle approaches 0°, the velocity profile becomes circulatory. Similar non-circulatory droplet formation hydrodynamics was recognized by Lu et al. [27]. Simulated and experimental formation times are shown in Table 4. For both needles experimental formation times $t_{F,m}$ mare somewhat larger compared to the simulated times $T_{F,LS}$. Experimental formation time was determined by dividing droplet feed rate with average droplet volume. The experimental error in formation time determination is 10%, for the 0.8 mm needle formation time is between 1.5 to 1.7 seconds and for the 0.4 mm needle between 1.2 to 1.6 seconds. Interfacial tension is affected by copper extraction [40,41]. When the interfacial tension is 25.5 mNm^{-1} the simulated formation times equals the experimental value for the 0.8 mm needle.

Droplet rise

Based on concentration measurements during a droplet rise (Figure 2) it was recognized that reacted copper complex has a tendency stay at the droplet bottom zone. This supports the assumption of stagnant cap model. Terminal velocity measurements Tamminen et al. [6] gave substantially smaller values than determined from correlations for pure systems which is due to the presence of surfactants i.e., extractant, reducing the interface mobility. Low value of the measured terminal velocity (113 mm/s) corresponds well with the correlation given by Grace et al. [40] for contaminated systems. Based on this it is assumed that the interface is rigid thus signaling a very low value of interface mobility parameter $k_{H,R}$.

Two coefficients are to be determined experimentally when stagnant cap model is combined with effective diffusivity: stagnant volume fraction f_v and contamination coefficient $k_{H,R}$. In this work f_v is determined with image analysis. $k_{H,R}$ was set to zero based on the rigid interface assumption.

Volume fractions of stagnant cap were estimated by measuring droplet major and minor axis lengths and height of stagnant cap from the droplet image. Cap boundary was visually recognized and can also be seen in concentration profiles (Figure 2). Determination was repeated at least 15 times in order to estimate the variation. Fractions are shown in Table 5.
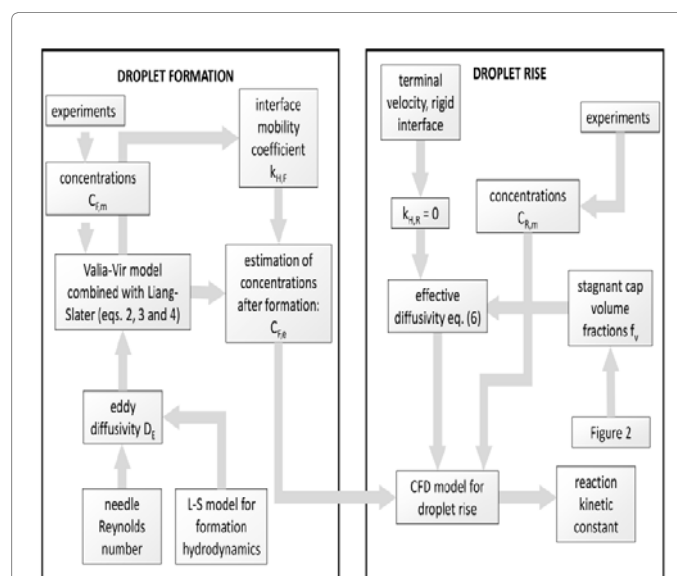

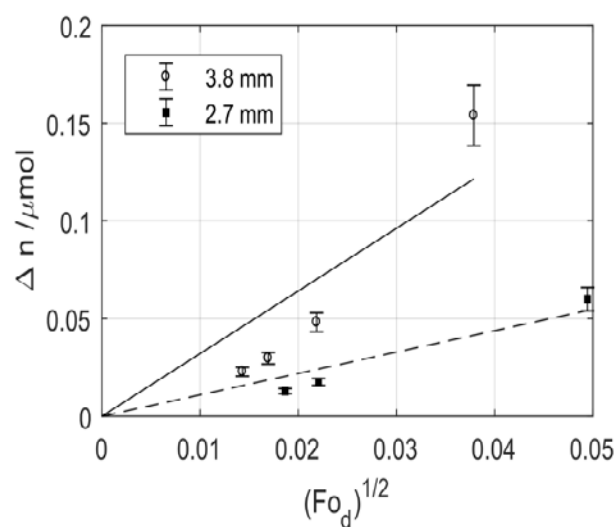**Figure 4:** Flow diagram describing the calculation and application mass transfer models.

Figure 5: Measured and estimated cumulative mass transfer Δn against the Fourier number and the cumulative transfer model by Popovich (eq. 1): 3.8 mm, 2.7 mm. Symbols refer to experimental values. The fitted value of coefficient a_1=0.35.

Mass transfer simulation using CFD was performed for 0.8 mm needle. It was assumed that $k_{H,R}$ does not depend on the feed rate Q. Droplet concentration $C_{F,e}$ after formation was estimated using the model presented in the section *Mass transfer in droplet formation*. Droplet terminal velocity U_t was set to experimental value 113 mm/s. Droplet diameter was 3.8 mm and rise time 2.3 s. Droplet acceleration to terminal speed was neglected because of a very short acceleration time.

Value for the kinetic constant $k_{R,A}$ was found by fitting with the CFD model. The sum of squared difference between the estimated and measured concentrations was minimized:
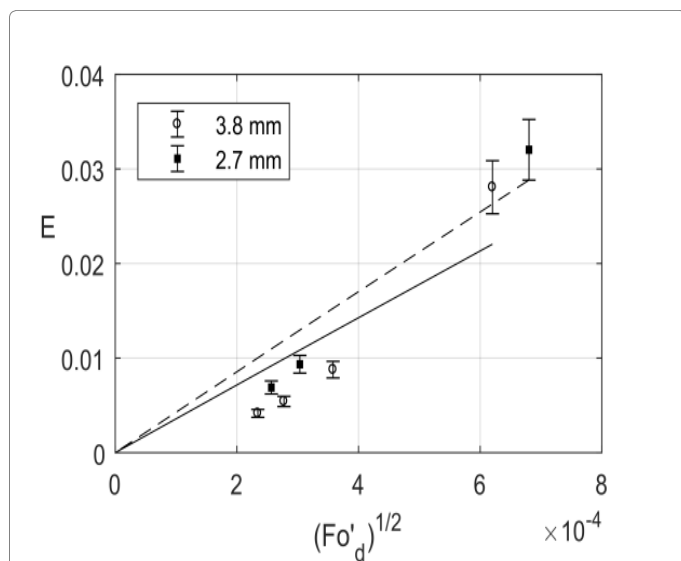
Figure 6: Measured and estimated extraction ratio E vs. square root of droplet modified Fourier number Fo'$_d$ (eqs 2 and 4): 3.8 mm, 2.7 mm. Symbols refer to experimental values. Correction factor k$_{H,F}$ due to surface mobility is approximately 0.07 for both droplet sizes.
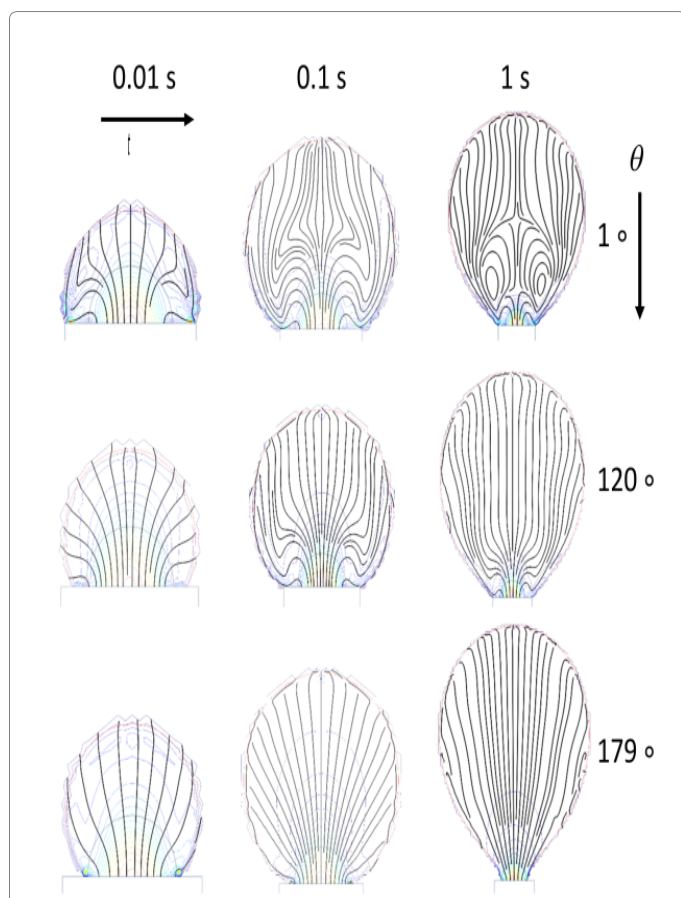

Figure 7: Simulated velocity profiles during droplet formation with different contact angles θ and different times. Feed rate Q is 1 ml/min and needle diameter 0.8 mm.

$$SSQ = \min\left(\sum_{j=1}^{4} \left(c_{R,m,j} - c_{R,e,j} \right)^2 \right) \qquad (14)$$

$C_{R,m,j}$ is measured concentration in j:th feed flow and $C_{R,e,j}$ is the estimated concentration calculated with the CFD model.

Fitted value of $k_{R,A}$ is 0.13×10^{-6} dm^4/(mol s). This is substantially smaller than reported by Tamminen et al. [38]. It is obviously due to different hydrodynamic conditions and smaller droplet size compared to this work. Estimated concentration after formation, and measured and estimated droplet concentrations after rise are shown in Table 5.

CFD model was used to calculate mass transfer coefficients using eqs. 12a-c. the most dense mesh (Table 6) was used. Mass transfer coefficients are K_d=0.7 × 10^{-6} m/s, k_{CuA2}=13 × 10^{-6} m/s and k_{Cu}=34 × 10^{-6} m/s. Average K_d estimated from experiments is 2 × 10^{-6} m/s. k_{CuA2} calculated from Newman model (eq. 8) with eddy diffusivity D$_{R,E}$=0 (rigid interface) is 13 × 10^{-6} m/s which is same magnitude compared to value provided by the CFD model. Cu mass transfer coefficient k_{Cu} in continuous phase is estimated with a correlation proposed by Clift et al. [1].

$$Sh_c = 1 + Re^{0.48}Sc_c^{1/3} \qquad (15)$$

With U_t=113 mm/s, d_e=3.8 mm, ρ_c=1020 kg/m^3, μ_c=1.1 mPas and D$_{cu}$=0.72 × 10^{-9} m^2/s, Re is 388, Sc_c=1498, Sh_c=146 and k$_{Cu}$=Sh$_c$D$_{Cu}$/d$_e$=28 × 10^{-6} m/s. This is slightly smaller than the value 34 × 10^{-6} calculated from CFD model.

Fractional mass transfer resistances for continuous phase (m/k_{Cu})/(1/K_d) is 2% and for droplet (1/k_{CuA2}) / (1/K_d) is 5%. Copper distribution ratio m between aqueous and droplet phase is 1.2. The reaction fractional resistance is 100%-7%=93% which is a substantial proportion of the total resistance. Similar results were also reported by Ferreira et al. [34].

Solution sensitivity for the selected mesh was tested by simulating using six meshes and calculating mass transfer coefficients (Table 6). Mass transfer coefficients are nearly constant when more than 1 × 10^6 mesh elements were used. Newman model assumes that mass transfer resistance is totally on the droplet side. Continuous side resistance is 2.5 times smaller than the droplet side but the reaction provides the

d$_n$	Q	t$_{F, LS}$	t$_{F,m}$	V$_m$	V (t$_{F,LS}$)	V$_{F,LS}$
mm	mL/min	S	s	mm³	mm³	mm³
0.8	1	1.3	1.7	26	22	19.4
0.4	0.41	1.1	1.4	9.5	8.3	7.8

Table 4: Comparison of calculated and experimental formation times and volumes for both needles with maximum feed rate Q. t$_{F,LS}$, droplet formation time in simulation t$_{F,m}$ experimental droplet formation time, V$_m$, experimental droplet volume, V(t$_{F,LS}$)=t$_{F,LS}$ × Q droplet volume at simulated formation time, V$_{F,LS}$ LS-method based droplet volume at the simulated droplet formation time t$_{F,LS}$.

Q	f$_v$	c$_{F,e}$	c$_{R,m}$	c$_{R,e}$
mL/min		mmol/dm³	mmol/dm³	mmol/dm³
0.1	0.39	4.1	5.1	4.6
0.3	0.25	2.3	2.5	2.8
0.5	0.23	1.8	2.1	2.3
0.7	0.25	1.5	2.1	2

Table 5: Stagnant cap fractions and estimated initial and measured and estimated final droplet copper complex concentrations. K$_{H,R}$=0 (=Rigid interface), estimated k$_{R,A}$=0.13 × 10^{-6} dm^4/(mol s). Symbols: Q feed rate, f$_v$, stagnant cap fraction, c$_{F,e}$ estimated concentration after formation, eqs. (2 and 3), c$_{R,m}$, measured average concentration after the rise, c$_{R,e}$, estimated average droplet concentration after the rise.

N_{elem}	K_d	k_{CuA2}	k_{cu}
	10^{-6} m/s	10^{-6} m/s	10^{-6} m/s
475000	0.6	15	50
670000	0.71	15	45
1060000	0.71	14	41
1300000	0.71	14	39
1580000	0.71	14	36
2240000	0.7	13	34

Table 6: Mass transfer coefficients using the CFD model with six meshes. Feed rate is 0.1 ml/min.

most of the resistance so validity to use only Newman model is not justified.

Conclusion

Based on simulation of a rising droplet using stagnant cap assumption and estimating an interfacial reaction kinetic constant it was found that value of measured kinetic constant with high shear reactors is much larger than estimated by simulation. This supports the hypothesis that in this case the interface provides a substantial mass transfer resistance which decreases the overall mass transfer coefficient. The effect is assumed to be due to the structure of the interface which is affected by the hydrodynamic conditions and in this case due to surfactants which probably is been adsorbed into the interface thus making it rigid and on the other hand slowing the reaction reactant's and product's mobility to and away the interface. For the formation stage as well it was found that an empirical model combined with effective diffusivity using interface mobility parameter to describe effect of surfactants is able to predict mass transfer in droplet formation better than a model assuming no explicit interfacial effects.

Acknowledgements

Notations

a_1	Coefficient in eq (1)
c	Concentration, M
D	Diffusion coefficient, m²/s
d	Diameter, m
d_e	Volume equivalent sphere diameter,
E	Extraction ratio
E_d	Extraction ratio assuming constant concentration,
f_v	Fraction of droplet stagnant zone
g	Gravitational acceleration, m/s²
h	Height of droplet, mm
i	Species label
K	Overall mass transfer coefficient, m/s
K_E	Equilibrium constant in extraction reaction rate equation
k	Local mass transfer coefficient, m/s
k_E	Empirical coefficient in pseudo-eddy diffusivity equation
k_H	Interface mobility parameter
$k_{R,A}$	Reaction kinetic constant, dm⁴/(mol s)
$K^o_{R,A}$	Experimental kinetic constant determined in high shear reactor, dm⁴/(mol s)

m	Partition coefficient, distribution ratio between the phases
n	Molar amount, mol
N_{elem}	Number of elements in CFD mesh
p	Pressure, pa
Q	Feed rate, ml/min
R_A	Reaction rate, mol/(dm² s)
R²	Coefficient of the determination for a fitted model
r	Radius, mm
t	Time, s
u	Radial velocity in cfd model, m/s
U	Velocity, m/s
V	Droplet volume, ml, mm³
w	Axial velocity in cfd model, m/s
x	Volume fraction
z	Summing index
SSQ	Sum of squared differences

Greek alphabet

a	Species stoichiometric coefficient
Δ	Difference
γ	Interfacial tension, n/m
k	Viscosity ratio, μ_d/μ_c
μ	Viscosity, pa s
ρ	density, kg/m³
Θ	Contact angle, degrees

Subscripts

-	Average
c	Continuous phase
d	Droplet
e	Estimated
E	Eddy diffusivity
Eff	Effective diffusivity
*	Equilibrium
F,c	Formation in cfd model
F	Formation
i	Interface, species index
LS	Levelset
Maj	Droplet major axis
Min	Droplet minor axis
m	Molecular, measured
N	Needle
R	Rise
0	Initial time, maximum value of reaction kinetic constant
t	Terminal velocity

Abbreviations

(aq)	Aqueous phase
CFD	Computational fluid dynamics
Cu^{2+}	Copper ion
CuA2	Copper complex
DNS	Direct numerical simulation
H^+	Proton
HA	Hydroxyoxime
(i)	Interface
i.d, o.d	Needle inner and outer diameters
LS	Levelset
LLE	Liquid-liquid extraction
(org)	Organic phase
SDS	Sodium dodecyl sulphate
VOF	Volume-of-fluid

Dimensionless numbers

Fo_d	Droplet fourier number, $4D_m t_F/d^2_e$
Fo'_d	Modified droplet fourier number, $4D_{F,eff} t_F/d^2_e$
Maj	Droplet major axis
Re	Droplet reynolds number, $Ud_e \rho_c/\mu c$
Re_N	Needle Reynolds number, $\bar{U}_n \rho_d d_n / \mu_d$
Sh_C	Continuous phase sherwood number, $k_c d_e/D_m$
SC_c	Continuous phase schmidt number, $\mu_c/(D_m \rho_c)$

References

1. Clift R, Grace JR, Weber ME (1978) Bubbles, Droplets and particles, Dover Publication, USA.

2. Licht W, Conway JB (1950) Mechanism of Solute Transfer in Spray Towers, Industrial & Engineering Chemistry 42: 1151-1157.

3. Licht W, Pansing WF (1953) Solute Transfer from Single Drops in Liquid-Liquid Extraction. Industrial and Engineering Chemistry 45: 1885-1896.

4. Liang TB, Slater MJ (1990) Liquid-liquid extraction drop formation: mass transfer and the influence of surfactant. Chemical Engineering Science 45: 97-105.

5. Wegener M, Paul N, Kraume M (2014) Fluid dynamics and mass transfer at single droplets in liquid/liquid systems. International Journal of Heat and Mass Transfer 71: 475-495.

6. Tamminen J, Lahdenperä E, Koiranen T, Kuronen T, Eerola T, et al. (2017) Determination of single droplet sizes, velocities and concentrations with image analysis for reactive extraction of copper. Chemical Engineering Science 167: 54-65.

7. Popovich AT, Jervis RE, Trass V (1964) Mass transfer during single drop formation. Chemical Engineering Science 19: 357-365.

8. Walia DS, Vir D (1976) Extraction from single forming drops. The Chemical Engineering Journal 12: 133-141.

9. Walia DS, Vir D (1976) Interphase mass transfer during drop or bubble formation, Chemical Engineering Science 31: 525-533.

10. Heideger WJ, Wright MW (1986) Liquid extraction during drop formation: Effect of formation time. AIChE Journal 32: 1372-376.

11. Kumar A, Hartland S (1999) Correlations for Prediction of Mass Transfer Coefficients in Single Drop Systems and Liquid-Liquid Extraction Columns. Chemical Engineering Research and Design 77: 372-384.

12. Newman AB (1931) The Drying of Porous Solid: Diffusions and Surface Emission Equations.Trans. Am. Inst. Chem. Eng. 27: 203-220.

13. Kronig R, Brink JC (1951) On the theory of extraction from falling droplets. Applied Scientific Research 2: 142-154.

14. Handlos AE, Baron T (1957) Mass and heat transfer from drops in liquid-liquid extraction. AIChE Journal 3: 127-136.

15. Henschke M, Pfennig A (1999) Mass-transfer enhancement in single-drop extraction experiments. AIChE Journal 45: 2079-2086.

16. Henschke M, Pfennig A (2002) Influence of sieve trays on the mass transfer of single drops. AIChE Journal 48: 227-234.

17. Altunok MY, Kalem M, Pfennig A (2012) Investigation of mass transfer on single droplets for the reactive extraction of zinc with D2EHPA. AIChE Journal 58: 1346-1355.

18. Slater MJ (1995) A combined model of mass transfer coefficients for contaminated drop liquid-liquid systems. The Canadian Journal of Chemical Engineering 73: 462-469.

19. Piarah WH, Paschedag AR, Kraume M (2001) Numerical simulation of mass transfer between a single drop and an ambient flow. AIChE Journal 47: 1701-1704.

20. Wegener M, Paschedag AR, Kraume M (2009) Mass transfer enhancement through Marangoni instabilities during single drop formation. International Journal of Heat and Mass Transfer 52: 2673-2677.

21. Jeon SJ, Pawelski A, Kraume M, Hong WH (2011) Mass transfer enhancement by the alkaline hydrolysis of ethyl acetate in a single droplet system. Journal of Industrial and Engineering Chemistry 17: 782-787.

22. Pawelski A, Jeon SJ, Hong WH, Paschedag AR, Kraume M (2013) Interaction of a homogeneous chemical reaction and mass transfer in a single moving droplet. Chemical Engineering Science 104: 260-268.

23. Deshpande KB, Zimmerman WB (2006) Simulation of interfacial mass transfer by droplet dynamics using the level set method. Chemical Engineering Science 61: 6486-6498.

24. Yang C, Mao ZS (2005) Numerical simulation of interphase mass transfer with the level set approach. Chemical Engineering Science 60: 2643-2660.

25. Kenig EY, Ganguli AA, Atmakidis T, Chasanis P (2011) A novel method to capture mass transfer phenomena at free fluid-fluid interfaces. Chemical Engineering and Processing: Process Intensification 50: 68-76.

26. Wang Z, Lu P, Wang Y, Yang C, Mao Z (2013) Experimental investigation and numerical simulation of Marangoni effect induced by mass transfer during drop formation. AIChE Journal 59: 4424-4439.

27. Lu P, Wang Z, Yang C, Mao ZS (2010) Experimental investigation and numerical simulation of mass transfer during drop formation. Chemical Engineering Science 65: 5517-5526.

28. Soleymani A, Laari A, Turunen I (2008) Simulation of drop formation in a single hole in solvent extraction using the volume-of-fluid method, Chemical Engineering Research and Design. ECCE 686: 731-738.

29. Lewis WK, Whitman WG (1924) Principles of gas absorption. Industrial and Engineering Chemistry 16: 1215-1220.

30. Krishna R, Taylor R (1986) Multicomponent Mass Transfer: Theory and Applications. In Handbook of Heat and Mass Transfer. Cheremisinoff NP (ed.), Volume 2: Mass transfer and reactor design. pp: 259-432.

31. Hu Y, Liu Z, Yuan X, Zhang X (2017) Molecular mechanism for liquid-liquid extraction: Two-film theory revisited. AIChE Journal 63: 2464-2470.

32. Adamson AW (1990) Physical Chemistry of Surfaces 5th Ed,Wiley, New York, USA, pp: 88.

33. Haynes WM (2017) CRC Handbook of Chemistry and Physics, 97th Edition CRC Press.

34. Ferreira AE, Agarwal S, Machado RM, Gameiro ML, Santos S, et al. (2010) Extraction of copper from acidic leach solution with Acorga M5640 using a pulsed sieve plate column. Hydrometallurgy 104: 66-75.

35. Reid CR, Prausnitz JM, Poling BE (1987) The properties of gases and liquids (4th Ed.) McGraw-Hill, USA.

36. COMSOL (2017) COMSOL Multiphysics V5.2.

37. Szymanowski J (2000) Kinetics and interfacial phenomena. Solvent Extraction and Ion Exchange 18: 729-751.

38. Tamminen J, Sainio T, Paatero E (2013) Intensification of metal extraction with high-shear mixing. Chemical Engineering and Processing: Process Intensification 73: 119-128.

39. Vasilyev F, Virolainen S, Sainio T (2017) Modeling the phase equilibrium in liquid-liquid extraction of copper over a wide range of copper and hydroxyoxime extractant concentrations. Chemical Engineering Science 17: 88-99.

40. Inoue K, Tsunomachi H, Maruuchi T (1986) Interfacial adsorption equilibria of a hydroxyoxime and its metal chelates. Journal of Chemical Engineering of Japan 19: 131-133.

41. Grace JR, Wairegi T, Nguyen TH (1976) Shapes and Velocities of Single Drops and Bubbles Moving Freely through Immiscible Liquids. Trans. Inst. Chem. Eng 54: 167-173.